

Review

Diazonium Gold Salts as Novel Surface Modifiers: What Have We Learned So Far?

Ahmad A. L. Ahmad ¹, Bizuneh Workie ² and Ahmed A. Mohamed ^{3,*}¹ Department of Chemistry, University of Maine, Orono, ME 04469, USA; ahmad.ahmad@maine.edu² Department of Chemistry, Delaware State University, 1200 DuPont HWY, Dover, DE 19901, USA; bworkie@desu.edu³ Center for Advanced Materials Research, Research Institute of Sciences and Engineering, University of Sharjah, Sharjah 27272, UAE

* Correspondence: ah.mohamed@sharjah.ac.ae

Received: 30 March 2020; Accepted: 13 April 2020; Published: 29 April 2020



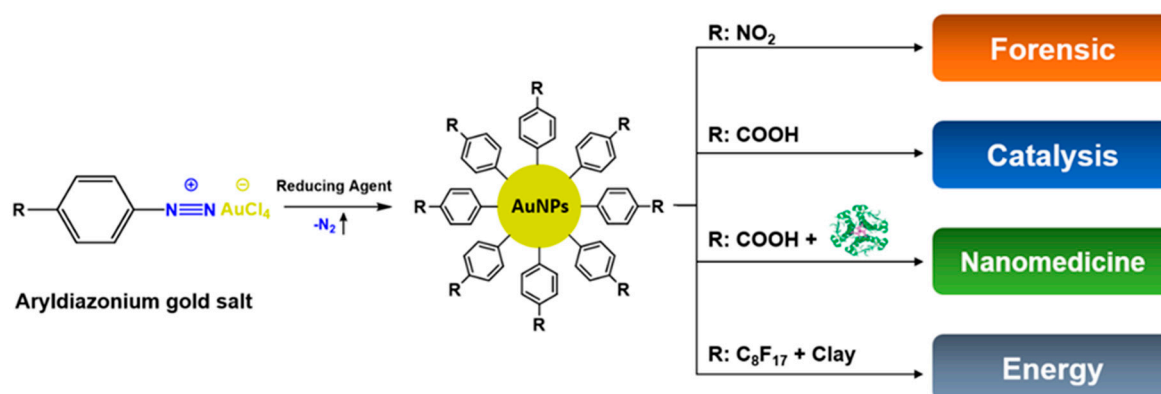
Abstract: The challenges of diazonium salts stabilization have been overcome by their isolation as metal salts such as tetrachloroaurate(III). The cleavage of molecular nitrogen from diazonium salts even at very low potential or on reducing surfaces by fine tuning the substituents on the phenyl ring expanded their applications as surface modifiers in forensic science, nanomedicine engineering, catalysis and energy. The robustness of the metal–carbon bonding produced from diazonium salts reduction has already opened an era for further applications. The integration of experimental and calculations in this field catalyzed its speedy progress. This review provides a narrative of the progress in this chemistry with stress on our recent contribution, identifies potential applications, and highlights the needs in this emerging field. For these reasons, we hope that this review paper serves as motivation for others to enter this developing field of surface modification originating from diazonium salts.

Keywords: diazonium gold salts; surface grafting; forensic nanotechnology; nanomedicine engineering; catalysis; energy

1. Introduction

Diazonium salts are outstanding surface modifiers at low electrochemical reduction potentials, chemical-less or even spontaneously [1–3]. The easily and rapidly formed salts particularly in the last few years could produce a wide variety of diazonium salts modified with functional groups such as amine, carboxyl, maleimide, boronic acid, thiol, and many others [2]. In 1992, Pinson and co-workers started one of the pioneering works to understand the mechanism of aryl radical attachment to glassy carbon electrodes [1]. The aryl–substrate interface with a true covalent bonding was a crucial step to use aryldiazonium salts as surface coupling agents and modifiers in material sciences for adhesive resins, biomacromolecules, polymers, optical sensing purposes, and nanoparticles for catalysis [2]. Scheme 1 shows aryldiazonium salts and their applications in several fields.

Preparation of aryldiazonium salts can be conducted from an aromatic amine in excess mineral acid media and addition of an aqueous solution of sodium nitrite which needs to be kept at a temperature below 5 °C. Aryldiazonium salts have many serious drawbacks in synthesis and stability: difficulty to purify and isolate, explosive nature, and substantial instability at room temperature [2,3]. To avoid these limitations, usually they are used in situ to the target application without isolation. For aliphatic diazonium salts, limited success in the synthesis of stable compounds has been reported because they are prone to release molecular nitrogen under experimental conditions [4].



Scheme 1. Preparation of gold nanoparticles from reducing aryldiazonium gold(III) salts with different examples of pendant groups that affect their properties and applications.

The two major routes to modify the nanoparticles are either using isolated or in situ generated aryldiazonium salts. Because of their ability to modify nanoparticles spontaneously, isolated aryldiazonium salts are highly interesting compounds to study. However, the long-term stability as solids and solutions has been a major concern. In situ generated aryldiazonium salts, instead of using isolated ones, can achieve high grafting densities of aryl layers with high colloidal stability. The robustness of aryl-capped gold nanoparticles can be at least for six months fabricated from in situ synthesized diazonium salts [5]. The ability to isolate pure and stable aryldiazonium salts plays an important factor in nanoparticles–aryldiazonium interface progress. However, various stable diazonium salts have been isolated and their X-ray structures have been reported [6,7]. For example, arenediazonium tosylates were prepared using a polymer-supported diazotization agent with *p*-toluenesulfonic acid. These salts showed outstanding stability that could be stored for long terms to use for subsequent transformation reactions [7].

2. Metal Nanoparticles Modification with Aryls from Aryldiazonium Salts

Metal nanoparticles modified with aryls from aryldiazonium salts can be prepared by one of these methods: (1) a spontaneous reduction of aryldiazonium salts on nanoparticles surface, (2) phase-transfer of aryldiazonium salts to metal salts, (3) reduction of aryldiazonium salts in the presence of metal salts, and (4) reduction of aryldiazonium salts bearing metal-based anions. We demonstrated in our group, for the first time, that we can synthesize stable diazonium tetrachloroaurate(III) salts [4-R-C₆H₄N₂]⁺AuCl₄⁻ (R = CN, C₈F₁₇, NO₂, F, Cl, Br, I, C₆H₁₃, water-soluble dendrons) in a high yield [8–10]. For example, protonation of 4-CN-C₆H₄NH₂ with H[AuCl₄] in water resulted in 4-CN-C₆H₄NH₂·AuCl₃, however, protonation in acetonitrile formed the anilinium tetrachloroaurate(III) salt [4-CN-C₆H₄NH₃]⁺AuCl₄⁻, which was easily oxidized by [NO]PF₆ to form a yellow diazonium tetrachloroaurate(III) salt [4-CN-C₆H₄N₂]⁺AuCl₄⁻. While the new diazonium salts stabilized with AuCl₄ are very stable, their handling in the laboratory must be manipulated with care. Metal spatulas must be avoided due to the spontaneous oxidization of the tool and the mixing of the clean salt powder with iron oxides. The sodium borohydride reduction of [4-C₈F₁₇-C₆H₄N₂]⁺AuCl₄⁻ in acetonitrile produced ruby red gold–carbon nanoparticles [9]. Functionalization of metal nanoparticles can be achieved by the attachment of organic shells with the desired functionality on their surfaces, which can affect the physical and chemical properties of the nanoparticles. Aryldiazonium modification of flat surfaces and nanoparticles occurs through direct metal–carbon, metal–oxygen–carbon, or metal–diazenido–carbon bonding. In addition, grafting depends on the nature of the metal surface and pre-treatment conditions [2].

Aryl shell can be adsorbed on metal oxide nanoparticles surfaces. However, in the case of MnO₂ nanorods modification Downard concluded from XPS studies on the in situ formed film from diazonium salts in acetonitrile solution or using isolated diazonium salt 4-nitrobenzenediazonium salt

in 0.1 M NaOH that covalent Mn-O-C bonding, through surface oxygen, to MnO₂ nanorods is formed. The possible formation of Mn-C bonds cannot be discounted [11].

Both the aryldiazonium salts chemistry and the photopolymerization iniferter methods were utilized in the synthesis of aluminum-carbon nanoparticles [12]. The functionalization of Al nanoparticles was performed by a bifunctional initiator, 4-[(diethylcarbamothioyl)thio] methylbenzenediazonium salt (DEDTC-CH₂-C₆H₄-N₂⁺), containing a diazonium end group for surface anchoring and a *N,N*-diethyldithiocarbamate (DEDTC) to activate surface-initiated photoiniferter-mediated polymerization (SIPIMP). Surface analysis shows that a thin aluminum oxide layer was preserved on the Al core and a strongly anchored organic shell surrounds it. XPS analysis of the modified Al nanoparticles showed the polymerization thickness over time reached 3–4 nm after 6 hrs. After functionalization, the oxide layer thickness decreased 57% and the C/Al atomic ratio increased progressively from 1.1 to 13.6, indicating an efficient coating by the polymer. Figure 1 testifies a clear enhancement of the metallic Al core contribution at ~72 eV relative to Al₂O₃ at ~75 eV in the presence of the aryl coating. Apparently, the diazonium approach has shown some restrictions due to the limited solubility of the diazonium salts in nonpolar solvents, preferred over polar protonated solvents, due to their inertness toward aluminum nanoparticles obtained from aluminum hydride.

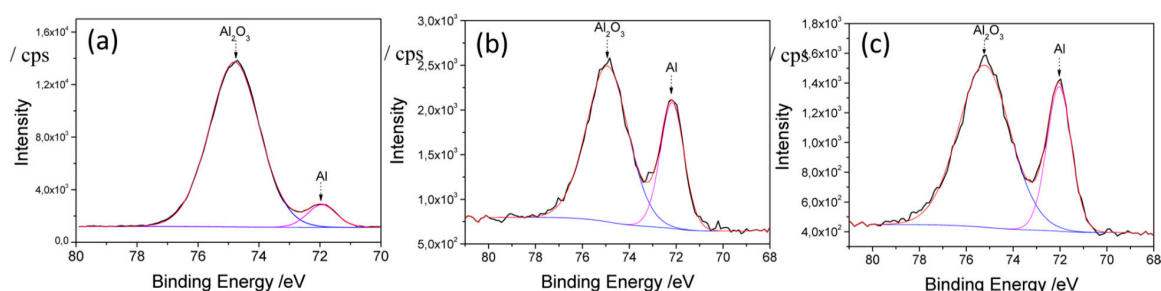


Figure 1. High resolution and peak fitting of Al₂p scans of (a) bare aluminum nanoparticles, (b) Al-4-[(diethylcarbamothioyl)thio] methylbenzenediazonium (DEDTC), and (c) Al-PMAA. Reprinted with permission from [12]. Copyright © 2020, American Chemical Society.

Trials by Nishihara and collaborators to utilize diazonium salts in vanadium modification produced diazenido (R-N=N-V) modified vanadium nanoparticles [13]. The construction of the nanoparticles was carried out by the reduction of VCl₄ with LiBHET₃ in the presence of 4-octylphenyldiazonium salt. XPS measurements provided clear evidence of the V-N bonding at approximately 396.5 eV. Recently, iron nanoparticles of 21 nm size were synthesized at room temperature by sodium borohydride reduction of iron(III) chloride in the presence of 4-nitrobenzenediazonium salt in an aqueous medium [14]. The synthesized nanoparticles maintained air stability and high oxidation resistance for at least 6 months.

3. Aryldiazonium Gold Salts for Flat and Nanoparticulate Surface Modification

Electrochemical reductive grafting of diazonium salts has been the privileged method for the modification of surfaces using aryl functional groups [15–24]. The reduction potential for the salts is very low, which aids in the modification process of a given surface without bringing further complications. Gold(III) diazonium salts showed a lower reduction potential on a glassy carbon electrode comparing with diazonium tetrafluoroborate [8]. The electrochemical reductive grafting works of the aryldiazonium gold(III) salts are in parallel with ongoing studies in the preparation of robust gold-organic nanoparticles, and the results provides rich foundation for covalent functionalization of gold surfaces [24]. Cyclic voltammetry (CV) studies of 1.0 mM of diazonium gold (III) salts of [4-X-C₆H₄N₂]⁺AuCl₄⁻, (X = F, Cl, Br, I, CN, NO₂ and C₈F₁₇), and bis(diazonium) gold(III) salts of syn- and anti-geometry of 4,4'-(1,3-phenylenediisopropylidene)bisaniline and of 4,4'-(1,4-phenylenediisopropylidene)bisaniline in 0.1 M tetrabutylammonium hexafluorophosphate-acetonitrile (TBAHFP-CH₃CN) showed highly irreversible reduction peaks at 100 mV/s scan rate in the range of

0.00 to -0.22 V vs. Ag/AgCl, KCl (satd.), both on the glassy carbon (GC) and platinum Pt working electrodes [21–24]. For all salts, multi cyclic voltammetry studies of ten consecutive cycles at both the GC and Pt working electrodes exhibited a decrease in the reduction current with an increase in the cycle number, and at the tenth cycle there is almost no reduction current validating that grafting and blocking of the gold–aryl film is complete. A typical case of the Br salt at GC electrode is shown in Figure 2.

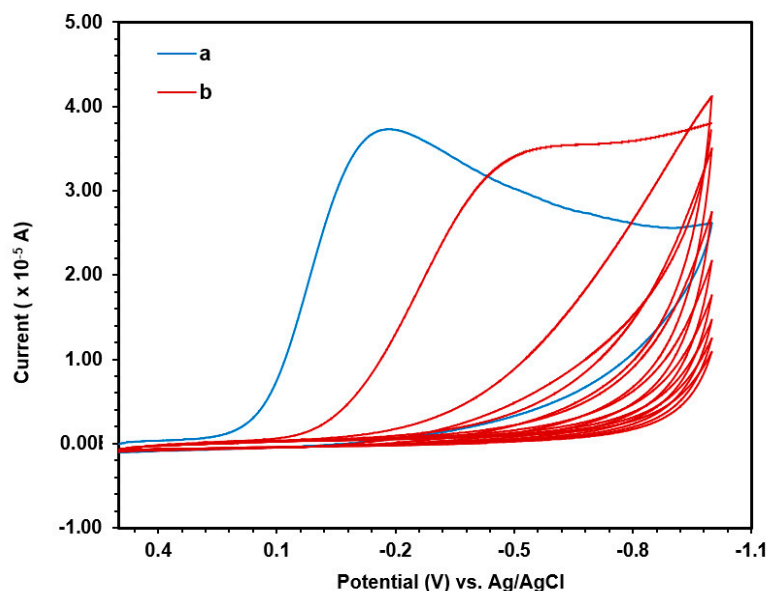


Figure 2. Cyclic voltammograms of 1.0 mM [Br-4-C₆H₄N≡N]AuCl₄ at a glassy carbon (GC) electrode in 0.1 M TBAHFP-CH₃CN (a) 1st run and (b) 2nd–10th runs at 100 mV/s scan rate. Unpublished result.

In order to determine the blocking efficiencies of the grafted films, CV studies of the reversible redox couple [Fe(CN)₆]^{3-/4-} were conducted using GC and Pt working electrodes prior and after grafting using 10 consecutive cycles in the potential range from 0.80 to -0.80 V vs. Ag/AgCl, KCl (satd.). For all [4-X-C₆H₄N₂]⁺AuCl₄⁻ salts, the redox peaks of [Fe(CN)₆]^{3-/4-} were completely attenuated due to the complete inhibition of its redox electron transfer by the grafted films on the GC working electrode. For the grafted films on the Pt electrode, the redox peaks of [Fe(CN)₆]^{3-/4-} were not disappearing, illustrating that the blocking and efficiency of the grafted film on Pt electrode is not as good as the GC electrode. Similar studies to check the robustness of the grafted films of all [4-X-C₆H₄N₂]⁺AuCl₄⁻ salts after one hour sonication in water, acetonitrile, toluene, water, and petroleum ether exhibited the grafted film on the GC electrode is robust. For the Pt electrode, except for petroleum ether, the grafted films were not found as robust as the GC films.

Similar [Fe(CN)₆]^{3-/4-} electron transfer and sonication experiments on the bis(diazonium) gold(III) salts of syn- and anti-geometry of 4,4'-(1,3-phenylenediisopropylidene)bisaniiline and of 4,4'-(1,4-phenylenediisopropylidene)bisaniiline using GC electrode showed that the grafted film for the syn diazonium salt is efficient and robust. The grafted film of the anti-salt on the GC electrode, however, was not found to be as efficient and robust as the syn salt. The grafted films on the Pt electrode for both the syn and anti bis(diazonium) gold(III) salts were found not to be efficient and robust.

Surface morphology studies conclude that the perfluorinated organic film C₈F₁₇-4-C₆H₄ was grafted on the in situ reduced gold(III) salt [4-C₈F₁₇-C₆H₄N₂]⁺AuCl₄⁻ [23,24]. ATR-FTIR shows the ν_{C-F} stretching frequencies of the perfluorinated film and the absence of the $\nu_{N\equiv N}$ stretching frequency for the diazonium peak. XPS study of the grafted film displays C1s peaks at 291–294 eV (CF₂/CF₃). The F1s and the C1s peaks testify for the successful electro-grafting of the fluorine group. Recent CV studies of [4-HOOC-C₆H₄N₂]⁺AuCl₄⁻ in 0.10 M KNO₃ aqueous solution showed a remarkably lower

irreversible reduction potential of 0.638 V vs. Ag/AgCl, KCl (satd.) than the other gold(III) diazonium salts, supporting its applicability in the synthesis of nanoparticles via green approach.

Femtosecond laser ablation of the aryldiazonium gold(III) salt was used in ultrapure gold–aryl nanoparticles construction in acetonitrile [25]. Also, the reduction of triazine dendrons as diazonium gold salts produced robust gold nanoparticles which are soluble in water and toluene [10]. Recently, the synthesis of aryldiazonium tetrachloroaurate(III) salts $[4\text{-X-C}_6\text{H}_4\text{N}_2]^+\text{AuCl}_4^-$ (X = F, Cl, Br, I, CN, NO₂) and their mild reduction to covalently functionalized nanoparticles was reported [26]. The gold–aryl nanoparticles were also constructed by the mild chemical reduction of the diazonium gold(III) salts. The study showed the presence of the gold(0) in the core and the organic shell connectivity in solid-state and in a solution using various spectroscopic techniques (see Figures 3 and 4). Furthermore, the experimental with theoretical results have been compared from Raman spectroscopy, which both supports the presence of gold–carbon bonding based on DFT calculations.

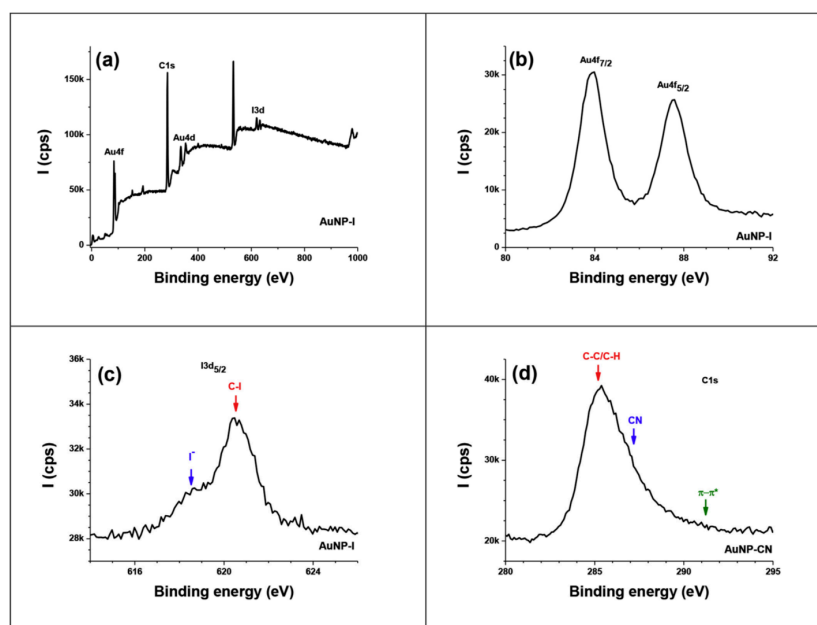


Figure 3. Typical XPS of AuNP-I (a–c) and AuNP–CN (d): survey spectrum (a), Au4f doublet (b), I3d_{5/2} (c), and C1s (d). Reprinted with permission from [26]. © 2020 Elsevier B.V. All rights reserved.

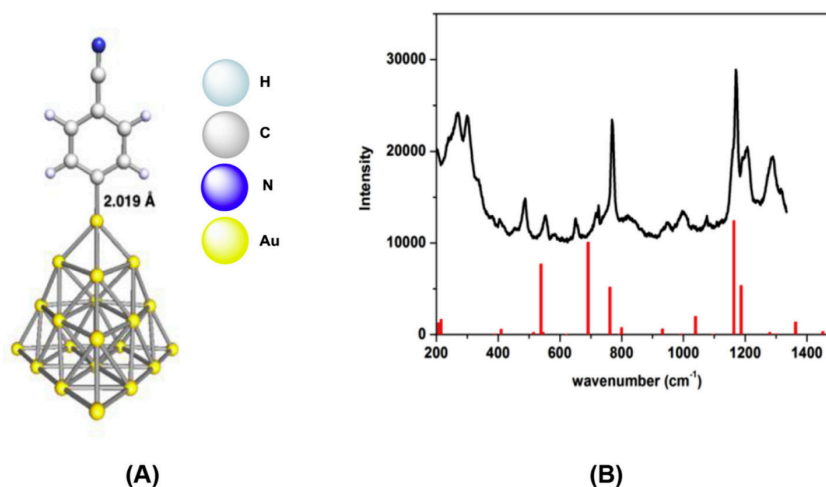


Figure 4. (A) DFT-optimized Au₂₀-C₆H₄-CN model in Cs symmetry and (B) experimental (black profile) and computed (red bars) Raman spectra for Au₂₀-C₆H₄-CN model. Reprinted with permission from [26]. © 2020 Elsevier B.V. All rights reserved.

4. Applications

4.1. Forensic Nanotechnology

Biological samples taken from crime scenes as evidence, such as fingerprints, elucidate more facts about the possible suspects and crime itself in the forensic investigations [27]. Latent fingerprints detection was developed rapidly include powdering [27,28], fluorescent imaging [29], visualization using polyelectrolytes [30], and cyanoacrylate fuming [31], scanning Kelvin probe [32], metal vapor deposition [33], and redox approaches for metal surfaces [34].

Diazonium salts can easily modify metal surfaces with organic film through electrochemical and electroless grafting methods [35]. Hence, using diazonium salts seems promising to use in crime scenes where it reacts preferentially on the reducing metal surface to generate fingerprints picture. Recently, aryldiazonium gold(III) salt was evaluated in forensic chemistry for latent fingerprint development on different metal surfaces. $[4\text{-NO}_2\text{-C}_6\text{H}_4\text{N}_2]^+ \text{AuCl}_4^-$ salt was applied with different concentrations to copper, lead, and aluminum surfaces using the components of human sweat as the reducing agent to construct gold deposits on the eccrine fingerprints [36].

The adsorbed gold–aryl film on the metal surfaces showed well-separated ridges of the latent fingerprints in the SEM measurements (Figure 5). Also, the presence of deposited gold helps to trace the fingerprint on the metal surfaces by XRF and EDS. Visualization of the developed fingerprints was studied by examining the primary, secondary, and tertiary details. Primary details can be obtained fully from the latent fingerprint on copper and lead surfaces. The secondary level is more important which gives more details for recognition like bifurcation, eye shape, island and ridge ends. The images show high quality on copper and lead surfaces due to the good contrast and clear furrows. Figure 6 shows the tertiary details as well. Overall, aryldiazonium gold(III) salt solutions produced a high-quality visualization of the latent fingerprints. The diazonium salts approach for metal surfaces modification allows the depositing gold metal that can be traced by XRF and EDS instruments compared to the electrochromism approach of polyaniline which depends on electrochemical handling [37].

Recently, we used XPS to investigate diazonium salts as surface modifiers of latent fingerprints collected on metal surfaces [38]. In this study, cleaned copper coins and copper sheets were modified by fingerprints of a donor. The fingerprints were developed with gold aryldiazonium ($[4\text{-NO}_2\text{-C}_6\text{H}_4\text{N}_2]^+ \text{AuCl}_4^-$) aqueous solution for 1 h. After washing, the copper coins and flat surfaces were analyzed by XPS. After only 15–20 min, the reaction of the diazonium aqueous solution with copper formed positive dark lines, and bubbles were visible between the fingerprint lines. Figure 7 shows XPS spectra collected from four different areas of the now-visible fingerprint samples. It was easy to differentiate the fingerprint side and the non-fingerprint side of the copper sample by looking at the survey scan and observing the shape of the background in the range of 700–900 eV. Only two peaks for nitrogen were observed, one centered at 400 eV and another at 406 eV assigned to $-\text{N}\equiv\text{N}-$ within the aryl layer and NO_2 , respectively. Therefore, the components due to $\text{N}1s$ from the diazonium group N_2^+ cannot be longer observed due to the spontaneous reduction of the diazonium cation on copper. $\text{Au } 4d_{5/2}$ accounts for the metallic state of gold and thus a reductive process affecting $[\text{AuCl}_4]^-$ anions. This combination of XPS and diazonium chemistry to study the development of latent fingerprints without any applied potential or heat offers fast application of fingerprint detection and development and can be further applied to other metal surfaces that have reducing properties.

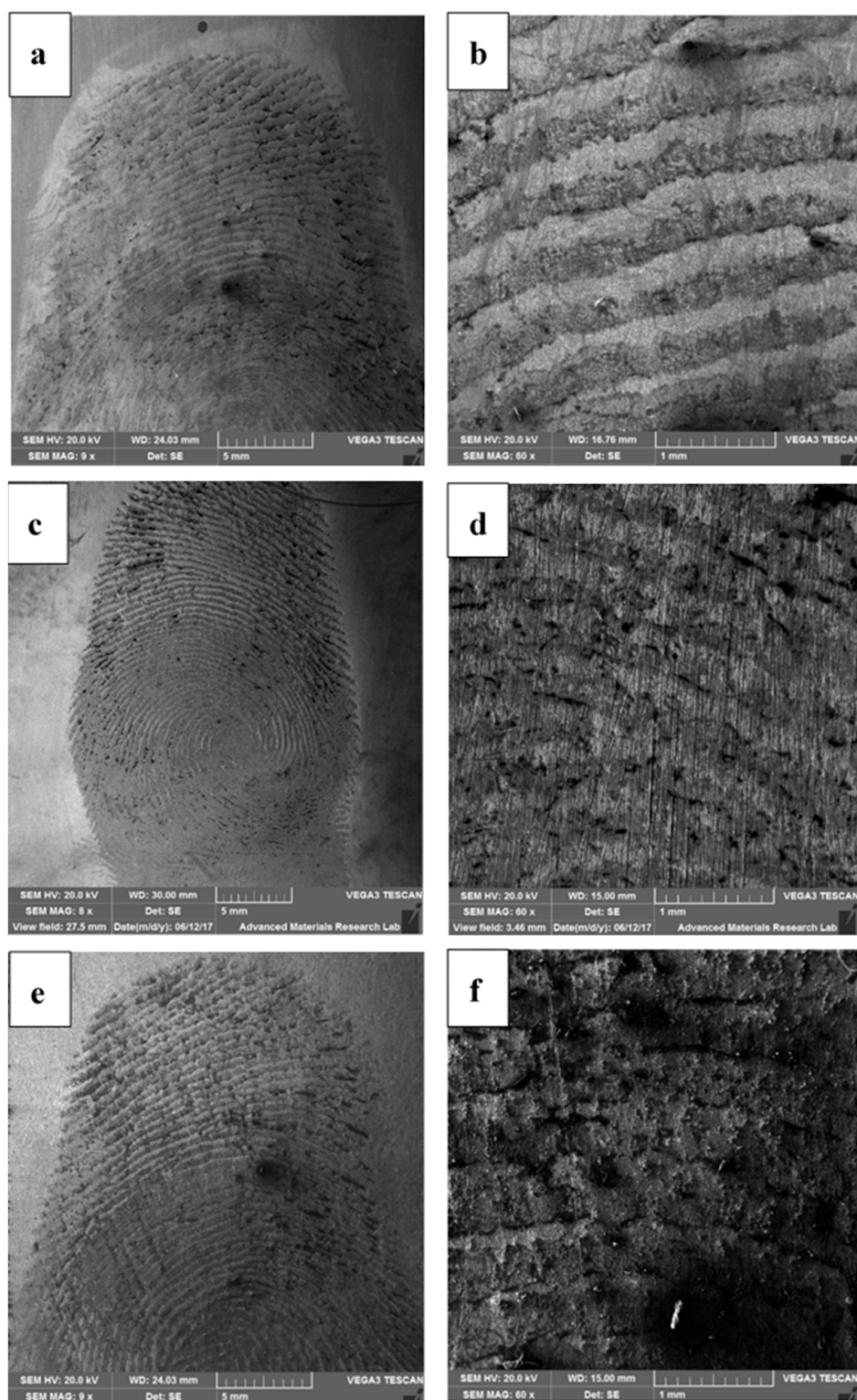


Figure 5. SEM images of (a,b) Cu, (c,d) Pb, (e,f) Al surfaces after spontaneous reduction of 0.001 M of $[4\text{-NO}_2\text{-C}_6\text{H}_4\text{N}_2]^+\text{AuCl}_4^-$ salt dissolved in 5% acetonitrile: 95% ethanol solvent after contact for 2 h with the latent fingerprints. Magnification: (a,c) 9 \times and (e) 8 \times . (b,d,f) 60 \times . Reprinted with permission from [36]. © 2020 Elsevier B.V. All rights reserved.

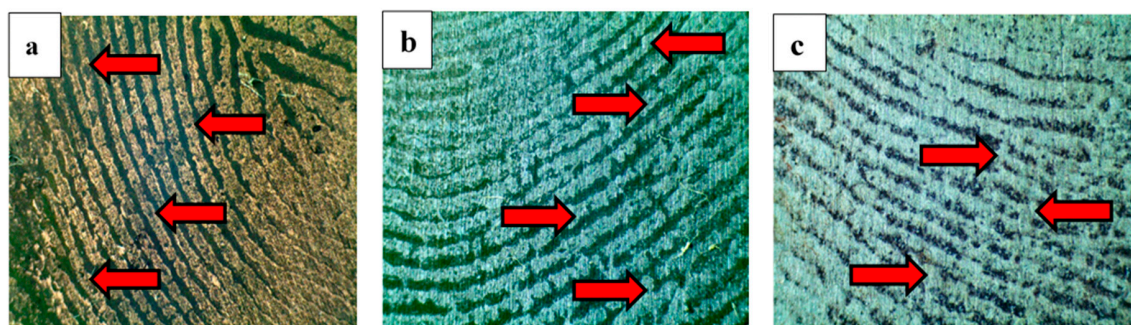


Figure 6. Tertiary details of fingerprints developed by 0.001 M of $[4\text{-NO}_2\text{-C}_6\text{H}_4\text{N}_2]^+\text{AuCl}_4^-$ salt dissolved in 5% acetonitrile: 95% ethanol solvent after contact for 2 h with (a) Cu surface showing incipient ridges, (b) Pb surface showing smooth edges and (c) Al surface showing some scar structures. Images were taken using stereomicroscope with a 3 MP camera and magnification of $25\times\text{--}50\times$. Reprinted with permission from [36]. © 2020 Elsevier B.V. All rights reserved.

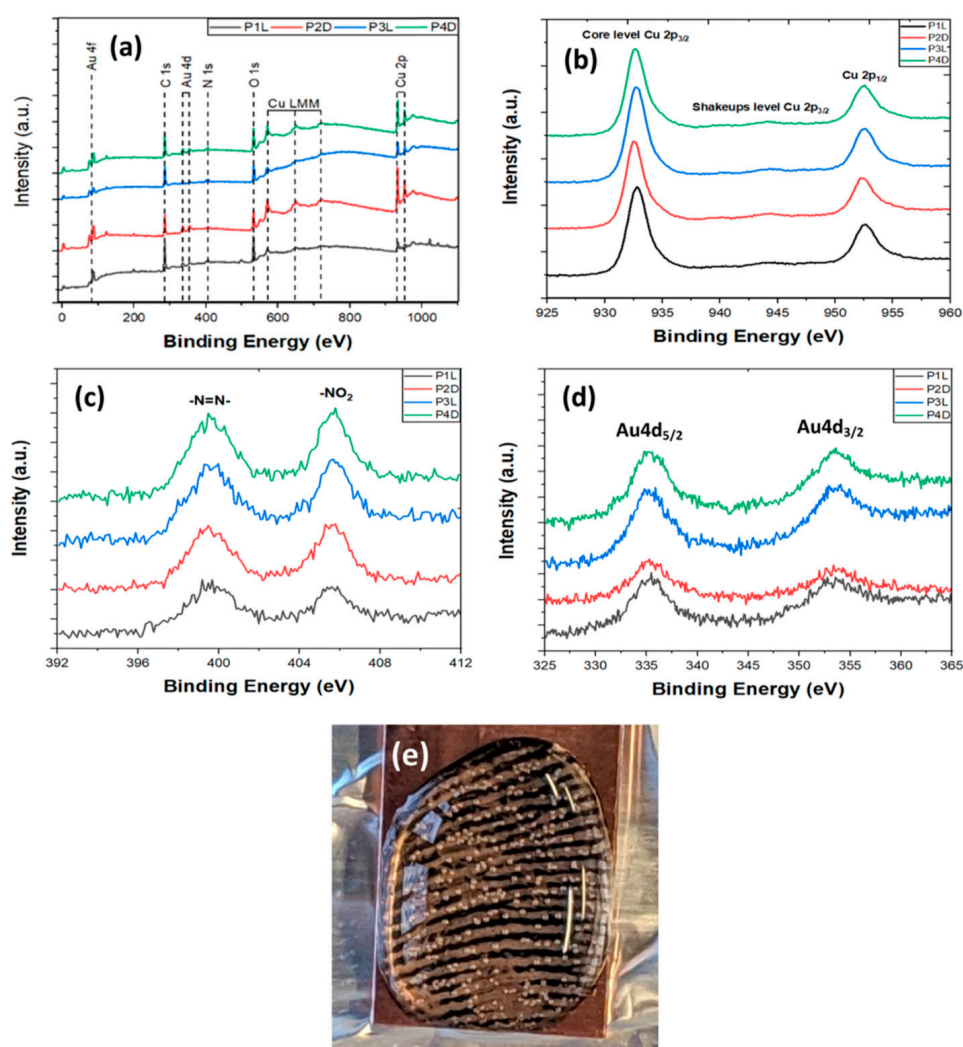


Figure 7. (a) XPS survey scan of a fingerprint and $[4\text{-NO}_2\text{-C}_6\text{H}_4\text{N}_2]^+\text{AuCl}_4^-$ treated copper sheet on four different areas; (b) high-resolution Cu 2p, (c) N 1s, and (d) Au 4d spectra; (e) latent fingerprint demonstration using diazonium solution on a copper sheet. Bubbles correspond to the release of N_2 due to the spontaneous reduction of the diazonium cation. Reprinted with permission from [38]. Copyright © 2020, American Chemical Society.

4.2. Catalysis

Water-soluble nanoparticles are important for several applications in medicine, catalysis, energy and environment [39–43]. The harsh conditions of these applications like the presence of salts, changing in pH values, and temperature variation requires robust nanoparticles that can maintain their composition. Aryldiazonium salts have been used to modify metal and nanoparticles surfaces [44]. The bonding between the aryl groups and the metal surface is very robust and can withstand harsh conditions such as ultrasonication and boiling in organic solvents [45]. The aryl film formed on the gold surface is very robust and opened a vast area for catalysis applications [46].

The modification of gold nanoparticles with an organic stabilizing robust shell using different aryldiazonium salts grafting method was previously reported [9]. For catalysis, water-soluble gold–aryl nanoparticles were prepared by the reduction of the aryldiazonium gold(III) salt, $[4\text{-HOOC-C}_6\text{H}_4\text{N}_2]^+\text{AuCl}_4^-$. The reduction of 4-nitrophenol (4-NPh) by sodium borohydride (NaBH_4) [47] was used to study the reactivity performance of gold–aryl nanoparticles (AuNPs-COOH) as a catalyst. Stability measurements showed high robustness of AuNPs-COOH under different catalytic conditions [48]. Overall, nanoparticles demonstrated high aggregation resistance in a wide pH range of 1–13. The ionic strength effect also studied using NaCl solutions (0.01–1.00 M) where the interaction of the nanoparticles with the ions in NaCl does not aggregate the nanoparticles completely. Thermal stability of functionalized nanoparticles is critical in catalytic applications. AuNPs-COOH stock solution was monitored by UV–Vis in the temperature range 20–90 °C. The nanoparticles also showed high stability with no redshift of the plasmon band in all studied temperature values.

DFT calculations estimate the gold–aryl binding energy in $\text{Au}_{38}\text{-C}_6\text{H}_4\text{-COOH}$ model with Cs Symmetry. The results agree well with the robust character with Au–C of 2.04 Å, which is related to the binding energy of -59.2 Kcal/mol. Comparing this result with the binding energy of thiol– Au_{38} model, Au–C shows a stronger and more stable bond than the Au–S bond. AuNPs-COOH used as a catalyst in the reduction of 4-NPh by NaBH_4 . The reduction reaction was monitored by UV–Vis spectrophotometer where the nitrophenolate ion has a strong band at 400 nm. Using an excess concentration of NaBH_4 , the reaction follows pseudo-first order kinetics. Figure 8 shows a rapid decrease in the intensity of the absorption peak at 400 nm, while there is an appearance of a new peak at 300 nm assigned to 4-aminophenol (4-APh). The reduction was complete in less than five minutes of 80 μM 4-NPh with a high k_{app} ($2.26 \times 10^{-2} \text{ s}^{-1}$). Activation parameters for the reduction reaction was also calculated. The AuNPs-COOH catalyst gives good values of $E_a = 25 \text{ kJ mol}^{-1}$, $H^\ddagger = 23 \text{ kJ mol}^{-1}$ and $S^\ddagger = -166 \text{ J mol}^{-1} \text{ K}^{-1}$.

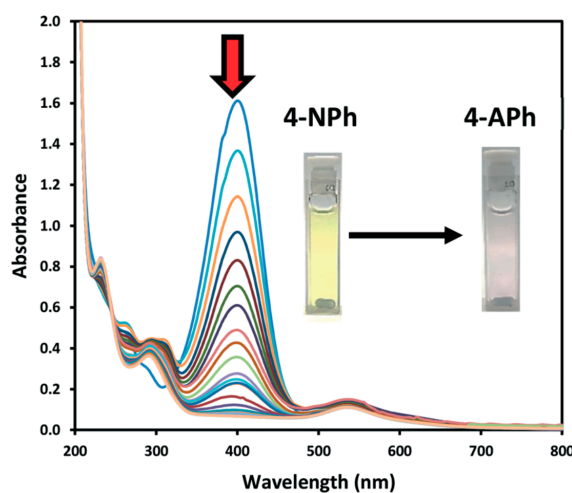


Figure 8. Reduction of 4-NPh with NaBH_4 in the presence of AuNPs-COOH recorded for 5 min ($[\text{NaBH}_4] = 0.024 \text{ M}$, $[4\text{-NPh}] = 80 \mu\text{M}$, and $[\text{Au}] = 38.0 \mu\text{M}$); the time between each scan is 12 s; inset photos show reduction reaction at time 0 and after 5 min. Reprinted with permission from [48]. Copyright 2019 The Royal Society of Chemistry.

4.3. Nanomedicine Engineering

Because of their facile surface functionalization, metal nanoparticles are dominating research studies in the biomedical field. Gold nanoparticles provide a plethora of prospects in theranostics due to their relatively biocompatible nature [49]. By using carboxylic-aryl shell modified gold nanoparticles, insulin could adsorb onto surface of the carboxylic groups [50]. The nanoparticles were synthesized by mixing the aryldiazonium gold(III) salt with insulin in the presence of mild reducing agents. Figure 9 shows the effect of pH gradient on color, zeta potential, plasmon peak position. The change in wavelength under reversible acidic-neutral-basic values was verified. From the graphs, even after two cycles of pH changes, acidic-neutral-basic, the reversibility is still obvious.

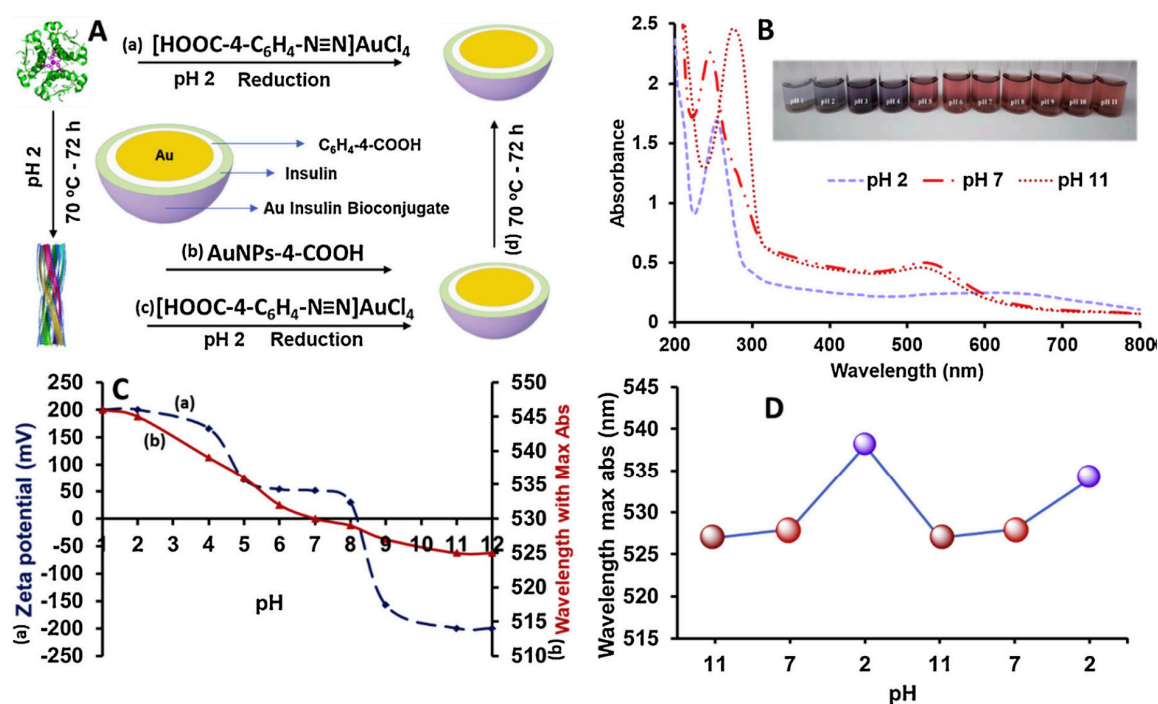


Figure 9. (A) Scheme showing different routes (a–d) for the fabrication of gold–insulin bioconjugate and the dissociation of amyloid fibrils in the presence of gold–aryl nanoparticles. (B) UV–vis examples of the change in the wavelength versus pH for the insulin bioconjugate. Inset showing color change over pH gradients. (C) pH effect on the insulin bioconjugate (a) zeta potential and (b) wavelength. (D) robustness study of the insulin bioconjugate under reversible change of pH of 2, 7 and 11. Change in color is represented as circles matching the visual color change upon reversible pH shift of two cycles between 2, 7 and 11. Reprinted with permission from [50]. © 2020 Elsevier B.V. All rights reserved.

Another gold bioconjugate was synthesized using bovine serum albumin (BSA) [51]. Because of the similar properties, molecular weight and amino acid sequence to human serum albumin, BSA has been widely used as model protein in bioconjugate fabrication. Using light and phase contrast microscopy, the morphology changes in blood cells and the percentage of hemolyzed cells were studied. The gold–aryl–COOH nanoparticles and Au–BSA bioconjugate showed a superior hemocompatibility probably because of the carboxyl groups.

In the presence of polyelectrolyte polymer, the interaction of aryl–gold nanoparticles with DNA was studied recently [52]. Gold–aryl nanoparticles were treated with biodegradable polydiallyldimethylammonium chloride (PDADMAC) as cationic polyelectrolytes. Nuclease degradation was reduced by DNA binding in the described bioconjugate, which increased its presence in the digestive environment of DNase-I enzyme. Binding and protection against nuclease degradation of DNA were studied using electrophoretic mobility of DNA in agarose gel. Figure 10 shows the bands of gold nanoparticles–DNA bioconjugate were the same as those of the native DNA, showing

no change in the electrophoretic mobility of DNA in the presence of unmodified gold nanoparticles. Immobilization of DNA was observed in the presence of PDADMAC–AuNPs, reflecting the efficient complexation of DNA by the cationic PDADMAC coated aryl–gold nanoparticles. The presence of a polymer PDADMAC masks the negative charge of the DNA and provide protection from enzymatic degradation.

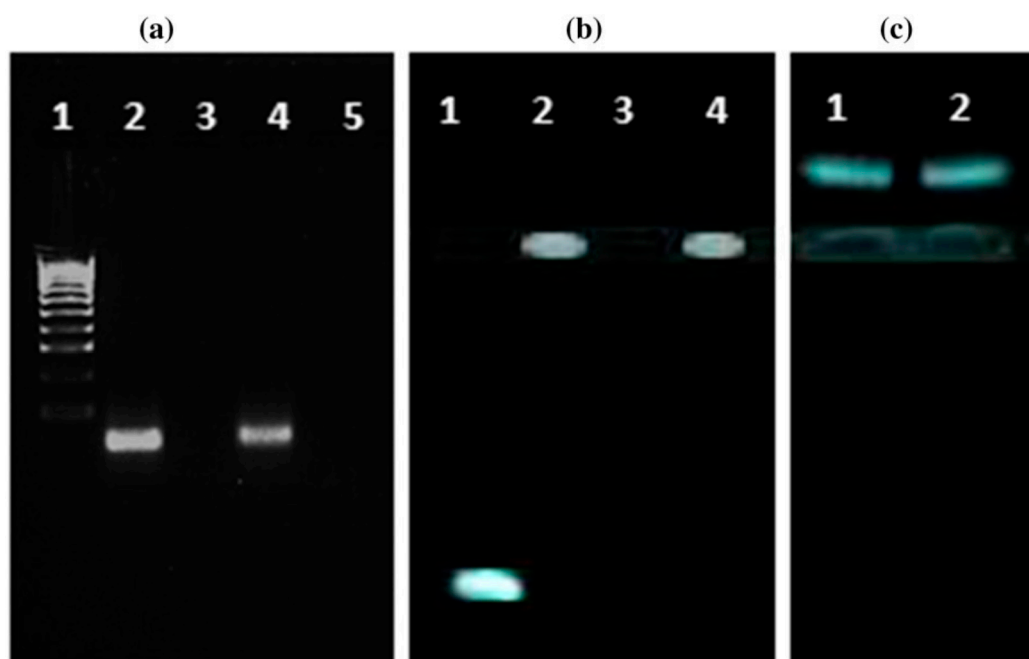


Figure 10. (a) Agarose gel electrophoresis image of DNase-I treated control DNA and AuNPs–DNA: Lane 1: DNA Ladder, Lane 2: Control DNA, Lane 3: control DNA treated with DNase-I (2 U/mL), followed by addition of 20 mM EDTA, Lane 4: AuNPs–DNA mixture and Lane 5: AuNPs–DNA mixture treated with DNase-I (2 U/mL), followed by addition of 5% SDS, (b) Agarose gel electrophoresis image of DNase-I treated control DNA and PDADMAC–AuNPs–DNA. Lane 1: Control DNA, Lane 2: DNA conjugated with PDADMAC–AuNPs, Lane 3: Control DNA treated with DNase-I (2 U/mL), Lane 4: PDADMAC–AuNPs–DNA conjugate treated with DNase-I and (c) Lanes 1 and 2: eluted DNA samples (PDADMAC–AuNPs–DNA and DNase-I treated PDADMAC–AuNPs–DNA) by spin column (GEN050/SC-215F). Both bands moved towards the cathode, showing the positive nature of the eluted DNA. The electrophoresis was conducted in 1.5% agarose gel as described in experimental details section. Reprinted with permission from [52]. © 2020 John Wiley & Sons, Ltd.

4.4. Energy Sector

Diazonium gold salts as bentonite clay surface modifiers in the energy domain for the electrocatalytic hydrogen production in hydrogen evolution reaction (HER) was described [42]. Mirkhalaf used nanostructured electrocatalysts based on diazonium salts immobilized on electrode surfaces and organic film templates for enhancing electrochemical reactions [53]. Diazonium gold salts with perfluorinated chain were used to modify clay surface by the chemical reduction to form clay–gold nanocomposite, Figure 11. The electrocatalytic properties of gold–aryl–clay nanohybrid as efficient and robust catalyst contributes to the ever-growing sustainable energy sector. Addition of gold enhanced the electrochemical hydrogen evolution with a noticeable high current density of -25 mA cm^{-2} at -1 V (vs Ag/AgCl).

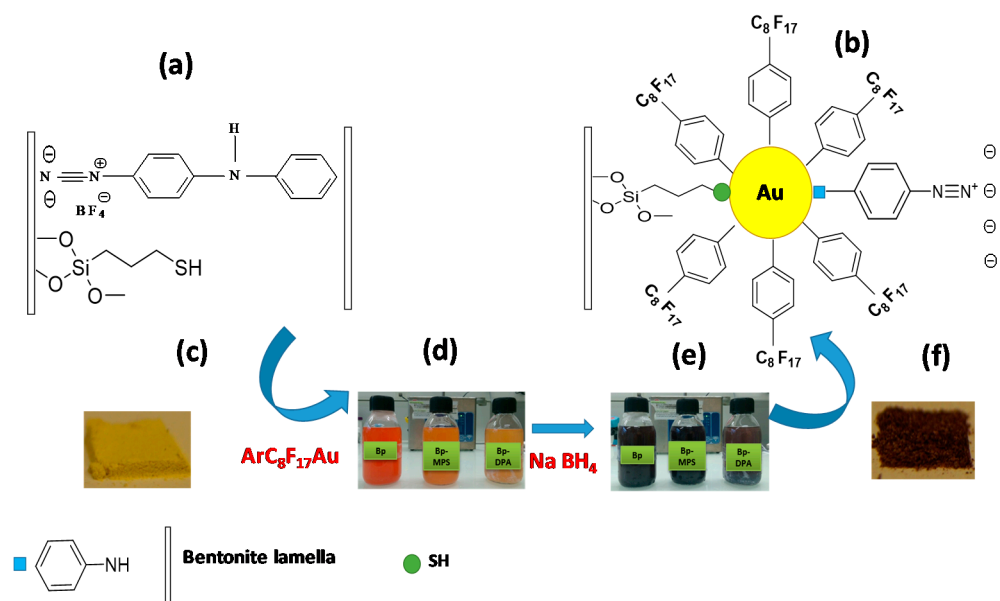


Figure 11. Upper panel: Preparation protocol of Bp-MPS-ArC₈F₁₇@Au § Bp-DPA-ArC₈F₁₇@Au (b) from the two pretreated bentonites by MPS coupling agent or by the DPA coupling agent (a). Lower panel: Digital photographs showing color change of Bp-MPS and Bp-DPA suspensions from yellow (d) to ruby (e) after reduction of gold nanoparticles on bentonite surface as well as the color change of the purified bentonite BP powder from greenish (c) to ruby (f) for both Bp-MPS-ArC₈F₁₇@Au and Bp-DPA-ArC₈F₁₇@Au prepared monohybrids. Reprinted with permission from [42]. © 2020 Elsevier B.V. All rights reserved.

5. Conclusions

Diazonium salts stabilized by metal-based anions are easily reducible. We utilized tetrachloroaurate salt to stabilize diazonium salts under ambient conditions. Gold(III) as a salt has added a few advantages such as the facile reducibility and the formation of gold–carbon of outstanding robustness. Moreover, the functionalization of the nanoparticles surface with different organics facilitated their applications in forensic science for latent fingerprints detection, nanomedicine engineering as protein carriers, catalysts in environmental pollutants removal and recently energy sector.

Author Contributions: Writing—original draft preparation, A.A.M.; writing—review and editing, A.A.L.A. and B.W.; funding acquisition, A.A.M. All authors have read and agreed to the published version of the manuscript.

Funding: This research was funded by the University of Sharjah support of SEED grant VC-GRC-SR-83-2015, competitive grants 160-2142-029-P and 150-2142-017-P, Organometallic Research Group grant RISE-046-2016 and Functionalized Nanomaterials Synthesis Lab grant 151-0039.

Conflicts of Interest: The authors declare no conflict of interest.

References

- Delamar, M.; Hitmi, R.; Jean Pinson, J.; Saveant, J.M. Covalent modification of carbon surfaces by grafting of functionalized aryl radicals produced from electrochemical reduction of diazonium salts. *J. Am. Chem. Soc.* **1992**, *114*, 5883–5884. [[CrossRef](#)]
- Chehimi, M.M. *Aryl Diazonium Salts: New Coupling Agents and Surface Science*; Editorial Wiley-VCH: New York, NY, USA, 2012; ISBN 978-3-527-32998-4.
- Mohamed, A.A.; Salmi, Z.; Dahoumane, S.A.; Ahmed Mekki, A.; Benjamin Carbonnier, B.; Chehimi, M.M. Functionalization of nanomaterials with aryldiazonium salts. *Adv. Colloid Interface Sci.* **2015**, *225*, 16–36. [[CrossRef](#)] [[PubMed](#)]

4. Doctorovich, F.; Escola, N.; Trapani, C.; Estrin, D.A.; Lebrero, M.C.G.; Turjanski, A.G. Stabilization of aliphatic and aromatic diazonium ions by coordination: An experimental and theoretical study. *Organometallics* **2000**, *19*, 3810–3817. [[CrossRef](#)]
5. Kesavan, S.; John, S.A. Fabrication of aminotriazole grafted gold nanoparticles films on glassy carbon electrode and its application towards the simultaneous determination of theophylline and uric acid. *Sens. Actuat. B-Chem.* **2014**, *205*, 352–362. [[CrossRef](#)]
6. Neal, S.N.; Orefuwa, S.A.; Overton, A.T.; Staples, R.J.; Mohamed, A.A. Synthesis of diazonium tetrachloroaurate(III) precursors for surface grafting. *Inorganics* **2013**, *1*, 70–84. [[CrossRef](#)]
7. Filimonov, V.D.; Trusova, M.; Postnikov, P.; Krasnokutskaya, E.A.; Lee, Y.M.; Hwang, H.Y.; Kim, H.; Chi, K.W. Unusually stable, versatile, and pure arenediazonium tosylates: Their preparation, structures, and synthetic applicability. *Org. Lett.* **2008**, *10*, 3961–3964. [[CrossRef](#)]
8. Overton, A.T.; Mohamed, A.A. Gold(III) diazonium complexes for electrochemical reductive grafting. *Inorg. Chem.* **2012**, *51*, 5500–5502. [[CrossRef](#)]
9. Orefuwa, S.A.; Ravanbakhsh, M.; Sabine, N.; Neal, S.N.; Julie, B.; King, J.B.; Ahmed, A.; Mohamed, A.A. Robust organometallic gold nanoparticles. *Organometallics* **2014**, *33*, 439–442. [[CrossRef](#)]
10. Enciso, A.E.; Doni, G.; Nifosi, R.; Palazzesi, F.; Gonzalez, R.; Ellsworth, A.A.; Coffey, J.L.; Walker, A.V.; Pavan, G.M.; Ahmed, A.; et al. Facile synthesis of stable, water soluble, dendron-coated gold nanoparticles. *Nanoscale* **2017**, *9*, 3128–3132. [[CrossRef](#)]
11. Bell, K.J.; Brooksby, P.A.; Polson, M.I.J.; Downard, A.J. Evidence for covalent bonding of aryl groups to MnO₂ nanorods from diazonium-based grafting. *Chem. Commun.* **2014**, *50*, 13687–13690. [[CrossRef](#)]
12. Atmane, Y.A.; Sicard, L.; Lamouri, A.; Pinson, J.; Sicard, M.; Masson, C.; Nowak, S.; Decorse, P.; Piquemal, J.Y.; Galtayries, A.; et al. Functionalization of aluminum nanoparticles using a combination of aryl diazonium salt chemistry and iniferter method. *J. Phys. Chem. C* **2013**, *117*, 26000–26006. [[CrossRef](#)]
13. Miyachi, M.; Yamamoto, Y.; Yamanoi, Y.; Minoda, A.; Oshima, S.; Kobori, Y.; Nishihara, H. Synthesis of diazenido-ligated vanadium nanoparticles. *Langmuir* **2013**, *29*, 5099–5103. [[CrossRef](#)] [[PubMed](#)]
14. Griffete, N.; Herbst, F.; Pinson, J.; Ammar, S.; Mangeney, C. Preparation of water-soluble magnetic nanocrystals using aryl diazonium salt chemistry. *J. Am. Chem. Soc.* **2011**, *133*, 1646–1649. [[CrossRef](#)] [[PubMed](#)]
15. Anariba, F.; DuVall, S.; McCreery, R. Mono- and multilayer formation by diazonium reduction on carbon surfaces monitored with atomic force microscopy “scratching”. *Anal. Chem.* **2003**, *75*, 3837–3844. [[CrossRef](#)] [[PubMed](#)]
16. Allongue, P.; de Villeneuve, C.; Cherouvrier, G.; Cortes, R.; Bernard, M. Phenyl layers on H/Si(111) by electrochemical reduction of diazonium salts: Monolayer versus multilayer formation. *J. Electroanal. Chem.* **2003**, *550–551*, 161–174. [[CrossRef](#)]
17. Kariuki, J.; McDermott, M. Formation of multilayers on glassy carbon electrodes via the reduction of diazonium salts. *Langmuir* **2001**, *17*, 5947–5951. [[CrossRef](#)]
18. Brooksby, P.; Downard, A. Multilayer nitroazobenzene films covalently attached to carbon. An AFM and electrochemical study. *J. Phys. Chem. B* **2005**, *109*, 8791–8798. [[CrossRef](#)]
19. Liu, G.; Bocking, T.; Gooding, J.J. Diazonium salts: Stable monolayers on gold electrodes for sensing applications. *J. Electroanal. Chem.* **2007**, *600*, 335–344. [[CrossRef](#)]
20. Finklea, H.O.; Avery, S.; Lynch, M.; Furtusch, T. Blocking oriented monolayers of alkyl mercaptan on gold electrodes. *Langmuir* **1987**, *3*, 409–413. [[CrossRef](#)]
21. Isah, S.; Workie, B.; Marcano, A.; Panicker, S.; Mohammed, A. Electrochemical reductive grafting and photothermal properties studies of bis(diazonium) gold(III) salts, Abstract of Papers. In Proceedings of the American Chemical Society 256th National Meeting, Boston, MA, USA, 19–23 August 2018.
22. Workie, B.; Mohammed, A. Electrochemical Reductive Grafting of studies of diazonium Gold(III) salts on glassy carbon electrodes, Abstract of Papers. In Proceedings of the American Chemical Society 254th National Meeting, Washington, DC, USA, 20–24 August 2017.
23. Neal, S.; Workie, B.; McCandless, B.; Mohammed, A. Surface morphology of the grafted perfluorinated gold-organic Film, Abstract of Papers. In Proceedings of the American Chemical Society 252nd National Meeting, Philadelphia, PA, USA, 21–25 August 2016.
24. Neal, S.; Workie, B.; McCandless, B.; Mohamed, A.A. Gold-organic thin films from the reductive grafting of diazonium gold(III) salts. *J. Electroanal. Chem.* **2015**, *757*, 73–79. [[CrossRef](#)]

25. Fernandez-Bravo, A.; Sivakumar, P.; Melikechi, N.; Mohamed, A.A. Femtosecond laser ablation synthesis of aryl functional group substituted gold nanoparticles. *J. Nanosci. Nanotechnol.* **2017**, *17*, 2852–2856. [[CrossRef](#)] [[PubMed](#)]
26. Mohamed, A.A.; Neal, S.N.; Atallah, B.; AlBab, N.D.; Alawadhi, H.A.; Pajouhafsar, Y.; Abdou, H.E.; Workie, B.; Sahle-Demessie, E.; Han, C.; et al. Synthesis of gold organometallics at the nanoscale. *J. Organomet. Chem.* **2018**, *877*, 1–11. [[CrossRef](#)]
27. Brunelle, E.; Huynh, C.; Le, A.M.; Halamkova, L.; Agudelo, J.; Halamek, J. New horizons for ninhydrin: Colorimetric determination of gender from fingerprints. *Anal. Chem.* **2016**, *88*, 2413–2420. [[CrossRef](#)] [[PubMed](#)]
28. Peng, D.; Wu, X.; Liu, X.; Huang, M.; Wang, D.; Liu, R. Color-tunable binuclear (Eu, Tb) nanocomposite powder for the enhanced development of latent fingerprints based on electrostatic interactions. *ACS Appl. Mater. Interfaces* **2018**, *10*, 32859–32866. [[CrossRef](#)]
29. Chen, Y.; Kuo, S.; Tsai, W.; Ke, C.; Liao, C.; Chen, C.; Wang, Y.; Chen, H.; Chan, Y. Dual colorimetric and fluorescent imaging of latent fingerprints on both porous and nonporous surfaces with near-infrared fluorescent semiconducting polymer dots. *Anal. Chem.* **2016**, *88*, 11616–11623. [[CrossRef](#)]
30. Yoon, J.; Jin, Y.; Sakaguchi, T.; Kwak, G. Visualization of sweat fingerprints on various surfaces using a conjugated polyelectrolyte. *ACS Appl. Mater. Interfaces* **2016**, *8*, 24025–24029. [[CrossRef](#)]
31. Xie, H.; Wen, Q.; Huang, H.; Sun, T.; Li, P.; Li, Y.; Yu, X.; Wang, Q. Synthesis of bright up conversion submicrocrystals for high-contrast imaging of latent-fingerprints with cyanoacrylate fuming. *RSC Adv.* **2015**, *5*, 79525–79531. [[CrossRef](#)]
32. Williams, G.; McMurray, N. Latent fingermark visualisation using a scanning Kelvin probe. *Forensic Sci. Int.* **2007**, *167*, 102–109. [[CrossRef](#)]
33. Davis, L.W.L.; Kelly, P.F.; King, R.S.P.; Bleay, S.M. Visualisation of latent fingermarks on polymer banknotes using copper vacuum metal deposition: A preliminary study. *Forensic Sci. Int.* **2016**, *266*, e86–e92. [[CrossRef](#)]
34. Bond, J.W.; Phil, D. Visualization of latent fingerprint corrosion of metallic surfaces. *J. Forensic Sci.* **2008**, *53*, 812–822. [[CrossRef](#)]
35. Mesnage, A.; Lefèvre, X.; Jégou, P.; Deniau, G.; Palacin, S. Spontaneous grafting of diazonium salts: Chemical mechanism on metallic surfaces. *Langmuir* **2012**, *28*, 11767–11778. [[CrossRef](#)] [[PubMed](#)]
36. Ahmad, A.A.L.; Alawadhi, A.H.; Park, J.; Abdou, H.E.; Mohamed, A.A. Evaluation of diazonium gold(III) salts in forensic chemistry: Latent fingerprint development on metal surfaces. *Forensic Chem.* **2019**, *13*, 100144. [[CrossRef](#)]
37. Beresford, A.L.; Hillman, A.R. Electrochromic enhancement of latent fingerprints on stainless steel surfaces. *Anal. Chem.* **2010**, *82*, 483–486. [[CrossRef](#)] [[PubMed](#)]
38. Almheiri, S.; Ahmad, A.A.L.; Droumaguet, B.L.; Pires, R.; Mohamed, A.A.; Chehimi, M.M. Development of latent fingerprints via aryldiazonium tetrachloroaurate salts on copper surfaces: An XPS study. *Langmuir* **2020**, *36*, 74–83. [[CrossRef](#)]
39. Lopes, T.S.; Alves, G.G.; Pereira, M.R.; Granjeiro, J.M.; Leite, P.E.C. Advances and potential application of gold nanoparticles in nanomedicine. *J. Cell. Biochem.* **2019**, *120*, 16370–16378. [[CrossRef](#)]
40. Thompson, D.T. Using gold nanoparticles for catalysis. *Nanotoday* **2007**, *4*, 40–43. [[CrossRef](#)]
41. Wu, Y.Y.; Mashayekhi, N.A.; Kung, H.H. Au–metal oxide support interface as catalytic active sites. *Catal. Sci. Technol.* **2013**, *3*, 2881–2891. [[CrossRef](#)]
42. Jlassi, K.; Zavahir, S.; Kasak, P.; Krupa, I.; Mohamed, A.A.; Chehimi, M.M. Emerging clay-aryl-gold nanohybrids for efficient electrocatalytic proton reduction. *Energy Convers. Manag.* **2018**, *168*, 170–177. [[CrossRef](#)]
43. Chaudhuri, R.G.; Paria, S. Core/shell nanoparticles: Classes, properties, synthesis mechanisms, characterization, and applications. *Chem. Rev.* **2012**, *112*, 2373–2433. [[CrossRef](#)]
44. Cao, C.; Zhang, Y.; Jiang, C.; Qi, M.; Liu, G. Advances on aryldiazonium salt chemistry based interfacial fabrication for sensing applications. *ACS Appl. Mater. Interfaces* **2017**, *9*, 5031–5049. [[CrossRef](#)]
45. Mirkhalaf, F.; Paprotny, J.; Schiffrin, D.J. Synthesis of metal nanoparticles stabilized by metal-carbon Bonds. *J. Am. Chem. Soc.* **2006**, *128*, 7400–7401. [[CrossRef](#)] [[PubMed](#)]
46. Chen, W.; Widawsky, J.R.; Vázquez, H.; Schneebeli, S.T.; Hybertsen, M.S.; Breslow, R.; Venkataraman, L. Highly conducting π -conjugated molecular junctions covalently bonded to gold electrodes. *J. Am. Chem. Soc.* **2011**, *133*, 17160–17163. [[CrossRef](#)] [[PubMed](#)]

47. Gu, S.; Wunder, S.; Lu, Y.; Ballauff, M.; Fenger, R.; Rademann, K.; Jaquet, B.; Zaccone, A. Kinetic analysis of the catalytic reduction of 4-nitrophenol by metallic nanoparticles. *J. Phys. Chem. C* **2014**, *118*, 18618–18625. [[CrossRef](#)]
48. Ahmad, A.A.L.; Panicker, S.; Chehimi, M.M.; Monge, M.; Lopez-de-Luzuriaga, J.M.; Mohamed, A.A.; Bruce, A.E.; Bruce, M.R.M. Synthesis of water-soluble gold-aryl nanoparticles with distinct catalytic performance in the reduction of the environmental pollutant 4-nitrophenol. *Catal. Sci. Technol.* **2019**, *9*, 6059–6071. [[CrossRef](#)]
49. Ridgway, Z.; Zhang, X.; Wong, A.G.; Abedini, A.; Schmidt, A.M.; Raleigh, D.P. Analysis of the role of the conserved disulfide in amyloid formation by human islet amyloid polypeptide in homogeneous and heterogeneous environments. *Biochemistry* **2018**, *57*, 3065–3074. [[CrossRef](#)]
50. AlBab, N.D.; Hameed, M.K.; Maresova, A.; Ahmady, I.M.; Arooj, M.; Han, C.; Workie, B.; Chehimi, M.; Mohamed, A.A. Inhibition of amyloid fibrillation, enzymatic degradation and cytotoxicity of insulin at carboxyl tailored gold-aryl nanoparticles surface. *Colloids Surf. A Physicochem. Eng. Asp.* **2020**, *586*, 124279. [[CrossRef](#)]
51. Hameed, M.K.; Ahmady, I.M.; Alawadhi, H.; Workie, B.; Sahle-Demessie, E.; Changseok Han, C.; Chehimi, M.M.; Mohamed, A.A. Gold-carbon nanoparticles mediated delivery of BSA: Remarkable robustness and hemocompatibility. *Colloids Surf. A Physicochem. Eng. Asp.* **2018**, *558*, 351–358. [[CrossRef](#)]
52. Panicker, S.; Ahmady, I.M.; Almehdi, A.M.; Workie, B.; Sahle-Demessie, E.; Han, C.; Chehimi, M.M.; Mohamed, A.A. Gold-Aryl nanoparticles coated with polyelectrolytes for adsorption and protection of DNA against nuclease degradation. *Appl. Organomet. Chem.* **2019**, *33*, e4803. [[CrossRef](#)]
53. Mirkhalaf, F.; Graves, J.E. Nanostructured electrocatalysts immobilised on electrode surfaces and organic film templates. *Chem. Pap.* **2012**, *66*, 472–483. [[CrossRef](#)]



© 2020 by the authors. Licensee MDPI, Basel, Switzerland. This article is an open access article distributed under the terms and conditions of the Creative Commons Attribution (CC BY) license (<http://creativecommons.org/licenses/by/4.0/>).